Treatment of Axial Data in Three-Dimensional PET

Margaret E. Daube-Witherspoon* and Gerd Muehllehner

Hospital of the University of Pennsylvania, Department of Radiology, Nuclear Medicine Section, Philadelphia, Pennsylvania

Improved axial spatial resolution in positron emission tomography (PET) scanners will lead to reduced sensitivity unless the axial acceptance angle for the coincidences is kept constant. A large acceptance angle, however, violates assumptions made in most reconstruction algorithms, which reconstruct parallel independent slices, rather than a three-dimensional volume. Two methods of treating the axial information from a volume PET scanner are presented. Qualitative and quantitative errors introduced by the approximations are examined for simulated objects with sharp boundaries and for a more anatomically realistic distribution with smooth activity gradients.

J Nucl Med 28:1717–1724, 1987

In multislice systems for positron emission tomography (PET), the problem of reconstructing a three-dimensional object is commonly separated into a set of two-dimensional problems by considering the object to consist of a series of parallel slices. The data used to reconstruct each slice are coplanar sets of line integrals through the volume with no data set containing object elements from other planes. In many detector geometries this assumption is justified, although the resultant photon utilization is low. To increase the sensitivity of some PET scanners, "cross-slices" are generated for which the line integrals involve elements from adjacent slices but are considered to be parallel to and midway between the "straight slices." This approximation avoids cumbersome and complicated reconstruction algorithms but can give rise to inaccuracies (*1,2*) including variations in the sensitivity with axial position and axial mispositioning errors.

If the axial resolution of a scanner is improved by reducing the axial acceptance angle (e.g., by reducing the axial extent of the detectors), the sensitivity will decrease. Alternately, if the acceptance angle is kept large as the axial extent of the detectors is reduced, the assumption of parallel projections through the object is no longer justified, and any improvement in axial resolution may be lost by mispositioning errors. More complicated, fully three-dimensional reconstruction algorithms must then be employed (*1,3–12*).

A multislice scanner for PET under construction at the University of Pennsylvania consists of six area NaI (Tl) crystals arranged in a hexagonal array, an extension of the prototype single-slice scanner (*13,14*). Because the scanner consists of area detectors, there will be almost continuous sampling in both the transverse and axial directions. A three-dimensional reconstruction would improve the axial quantitative accuracy by avoiding partial volume effects and would eliminate mispositioning errors inherent in discrete slice reconstruction.

To avoid the loss of resolution due to inadequate sampling, there are 12,500 sampling elements per detector (*15*). For the maximum axial acceptance angle the number of possible coincidence directions (projections) is on the order of 400 million for the scanner. Since the number of counts in a complete volume image will be on the order to 20–50 million, the data will be very sparsely distributed among these possible projections. The number of possible coincidence pairs imposes a severe requirement on the memory capabilities of the computer and makes it impossible practically to acquire three-dimensional projection data without a significant loss of information. If the data are backprojected directly into a three-dimensional image volume event-by-event, the memory requirements are reduced dramatically, since a matrix size of 128 × 128 × 50 will adequately sample most objects. Thus, the backprojected data will be contained in ~820,000 voxels, significantly reducing the size of the reconstruction prob-

Received Oct. 6, 1986; revision accepted May 28, 1987.

For reprints contact: Margaret E. Daube-Witherspoon, PhD, Nuclear Medicine Department, Clinical Center, Building 10, National Institutes of Health, Bethesda, MD 20892.

* Present address: The National Institutes of Health, Bethesda, MD.

lem. There exist several Fourier-based three-dimensional reconstruction algorithms which will reconstruct the object distribution given the back-projected data (*3,6–8*). However, these methods typically require a spatially invariant PSF. An iterative image space reconstruction algorithm (ISRA) has been developed (*2*) which uses the backprojected data image as input and is useful in cases where the computationally simpler technique of Fourier-based reconstruction is not applicable because the PSF is not spatially invariant.

Two methods of dealing with the axial information when backprojecting prior to reconstruction have been studied. This paper examines the errors in the reconstructed images if the axial projection angle is not treated properly either during backprojection or during the reconstruction. The first method consists of forming two-dimensional projection data by ignoring the axial projection angle as is currently done in multislice PET scanners. The second method consists of an event-by-event backprojection of the data through the three-dimensional image volume. In both methods a two-dimensional reconstruction algorithm is then used, and the acceptance angle is not restricted in the axial direction to avoid the loss of sensitivity which this restriction would entail.

RECONSTRUCTION TECHNIQUES

Two-Dimensional Projection Method

A common method for compressing coincidence data in scanners with multislice capability is to reorganize the data into a series of arrays of projection data, or sinograms, with projection data matrices corresponding to parallel slices through the object. A method of retaining the simplicity of a sinogram in three-dimensional imaging is depicted in Figure 1A. A coincidence event within the axial acceptance angle is assumed to have arisen from a parallel plane midway between the axial points of interaction of the two gamma rays in the detectors. This approach results in the generation of a series of two-dimensional projection matrices in which all projections are assumed to be parallel.

The two-dimensional sinogram method is similar to the technique of cross-slice generation in conventional multislice scanners with coincidences permitted not only between adjacent axial resolution elements but between a larger number of axial resolution elements up to an acceptance angle determined by either scatter shields or the axial extent of the scanner. Thus, the acceptance angle, slice thickness, and axial resolution are treated as separate parameters which are not in a fixed relationship to each other. The dominant factors determining the acceptance angle are the desired sensitivity and scatter fraction. Axial resolution is determined by the detector size or, in continuous detectors, by the spatial resolution of the detector in the axial direction, while the slice thickness is determined partly by the axial resolution and partly by the desired statistical accuracy.

The main advantage of the two-dimensional projection approximation is its simplicity. Having the data in the form of parallel projection data also allows one to use a variety of reconstruction techniques in addition to the ISRA algorithm. The data are reconstructed as a set of independent two-dimensional images with a total volume reconstruction time equal to the single-slice reconstruction time multiplied by the number of slices.

Event-by-Event Backprojection Method

The two-dimensional projection technique of treating the axial data is a rather crude approximation and might be expected to give rise to severe quantitative and qualitative errors, since the projections include data which originated several slices away. A second technique, shown in Figure 1B, is to backproject the coincidence data event-by-event taking the axial angle of each event accurately into account.

During the backprojection process the two points of intersection of the line connecting the detector coordinates with the sides of the backprojection volume are determined. Using a simple ray-tracing technique, points are calculated at equal distances along the ray within the back-projection volume, and the X, Y, Z coordinates of each point are truncated. The content of the memory location corresponding to this truncated point is incremented by "one." This technique assures equal projected density along the path and avoids time-consuming calculations involving the volume of overlap between each element and a cylindrical volume surrounding the ray, as is sometimes done in two-dimensional backprojection (*16*). It should be noted that along a backprojected ray some

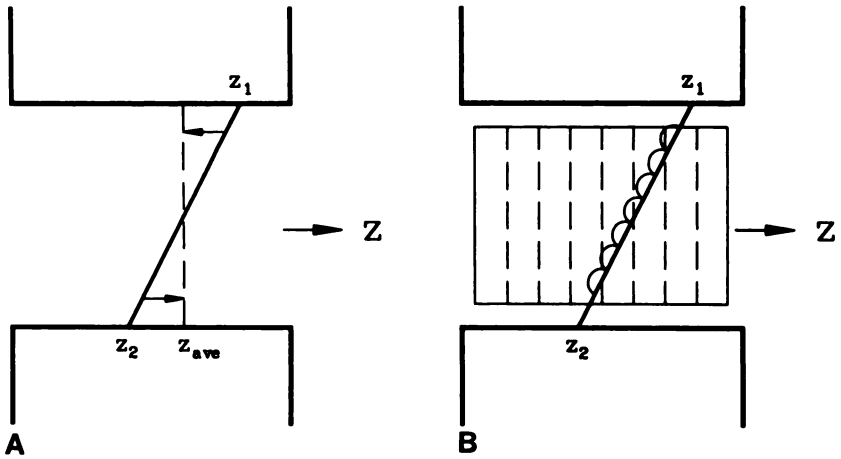

FIGURE 1
A: Two-dimensional projection method of compressing axial information. A coincident photon pair is assumed to have originated in a plane oriented perpendicular to the z-axis and located midway between the axial points of interaction of the two photons in the detectors. B: Event-by-event backprojection approach to axial data. A coincidence is accurately backprojected through a volume. During reconstruction the axial slices of the backprojection volume are treated as a set of parallel, independent, two-dimensional data.

memory locations may be incremented twice, particularly if the ray traverses the backprojection volume along a diagonal. This simple form of backprojection would certainly give rise to artifacts, if the backprojected quantity were a measured density. Since, however, the backprojection is carried out for each individual event and since the number of possible projection lines is large relative to the number of events backprojected (i.e., the probability of two events along the same projection line is low), this approach of selecting the nearest element leads to artifact-free backprojected images for all objects tested.

The most accurate method of reconstructing an image from the backprojected data would be a fully three-dimensional reconstruction algorithm. Currently available three-dimensional reconstruction algorithms either require a spatially invariant PSF or are computationally very expensive (*17*). We therefore examined the quantitative and qualitative inaccuracies which are introduced if the backprojected data are reconstructed using an image space reconstruction algorithm such as the ISRA algorithm, while treating the axial slices completely independently, as if the backprojected data in a slice came only from rays lying within and parallel to that slice, although the initial backprojection is performed accurately as described above. This technique leads to a set of two-dimensional backprojected data images to be reconstructed independently with a total volume reconstruction time again equal to the single-slice reconstruction time multiplied by the number of slices. Because the event-by-event backprojection process is computationally expensive (1.5 hr/million events on a VAX 11/780), a dedicated backprojector would be required for routine use of this method.

Computer Simulations

Data from the multislice PENN-PET scanner under construction were simulated on a VAX 11/780. The simulated objects include a box with dimensions 17 × 17 × 1 mm, a single 2-mm thick slice (12 × 15 cm transverse size) representing the distribution of fluorodeoxyglucose in a normal brain, generated by digitizing the Hoffman brain phantom (Data Spectrum Model 8080), and a complex set of spheres of varying radii and axial and transverse positions. The box and the brain slice were oriented with their thinnest side along the scanner z-axis; the box was positioned at several transverse locations (Fig. 2A). The sharp axial boundaries of these two objects represent worse-case situations, since objects with sharp axial gradients would be expected to be susceptible to artifacts generated by an approximate treatment of the axial data. Because few anatomic structures have sharp axial boundaries perpendicular to the body axis, the simulated sphere phantom was designed as a more realistic distribution of activity with smooth axial gradients and many, potentially interfering structures (Fig. 2B). All simulations were performed under ideal conditions (e.g., close to infinite statistics, perfect detector resolution, no effects from attenuation, scatter or random coincidences, no gaps at the corners of the hexagonal scanner). For all cases an axial acceptance angle of 13° was chosen, corresponding to the acceptance of all coincident events between the area detectors. This acceptance angle is approximately twice that of a typical multi-ring scanner which accepts coincident data from adjacent rings of detectors.

The results of the simulation studies were evaluated by several methods. First, the visual image quality was examined for thin (2 mm) slices to assess qualitative artifacts in the

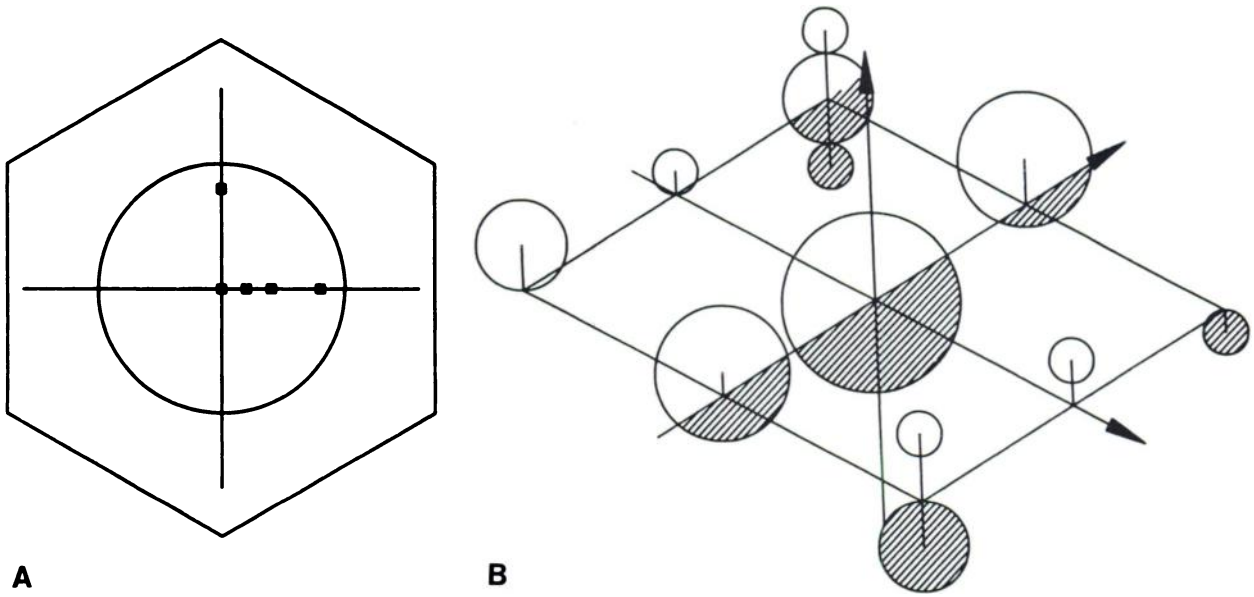

FIGURE 2
A: Transverse locations of simulated box phantom in PENN-PET volume scanner. The 17 × 17 × 1 mm box was centered at (X, Y) = (0 cm, 0 cm); (5 cm, 0 cm); (10 cm, 0 cm); (20 cm, 0 cm); and (0 cm, 20 cm). B: Schematic diagram of simulated complex sphere phantom. The vertical axis corresponds to the z-axis of the scanner. Shaded areas represent those portions of spheres located below (behind) the central slice of the scanner. The sphere diameters were 10 mm, 20 mm, 30 mm, and 40 mm. The maximum transverse offset of the center of a sphere from the center of the scanner was 64 mm.

images. Second, the fraction of total volume image counts and the maximum voxel count in thin slices were plotted against axial position and compared with the known distribution to quantitate axial smearing arising from mispositioning errors. To examine transverse smearing artifacts and loss of quantitative accuracy in the box simulations, regions of interest well within the border of the object were also drawn and the count densities plotted as a function of transverse position of the objects in the scanner.

RESULTS

Box

The images resulting from the simulation of a 17 × 17 × 1 mm thick box are shown in Figure 3 for 2-mm wide slices. The slice of highest intensity is centered upon the object. The images created with the two-dimensional projection method show considerable axial and transverse smearing which worsen with increased radial distance of the box from the center of the scanner. At 10 cm from the scanner axis, the 1-mm wide box is seen through an axial distance of more than 12 mm (Figs. 3D and 3E). The images generated with the event-by-event backprojection technique show little dependence on transverse position, and at 20 cm from the center of the scanner, the events are mostly contained in a single 2-mm slice although a faint "halo" of activity is seen in several other slices.

A plot of the fraction of total volume image counts in a 2-mm slice as a function of slice location is given in Figure 4. With the two-dimensional projection approach, as the box is moved radially outward from the center of the scanner, the counts are lost from the proper slice into slices at axial positions far removed from the correct location. The profiles obtained using the event-by-event backprojection approximation are unchanged with transverse position of the box. The counts in the "halo" of activity seen in neighboring slices to the central slice are <5% of the total counts in the volume image.

While the plot of the fraction of total volume counts as a function of slice gives one indication of axial smearing of the data, the overall effect of this smearing upon the quantitative accuracy and image quality will depend on how the events in the incorrect slice are distributed. A uniform, low-intensity background may be less troublesome than structured areas of high intensity. With the two-dimensional projection method, as the object is moved radially off-center, the maximum voxel intensity in neighboring slices becomes increasingly larger; at a radial distance of 10 cm off-axis, the maximum intensity in the adjacent slices is equal to the maximum voxel intensity in the proper slice. For the event-by-event backprojection method, the maximum intensity of the "halo" of activity in neighboring slices is <10% of the maximum voxel intensity in the correct slice.

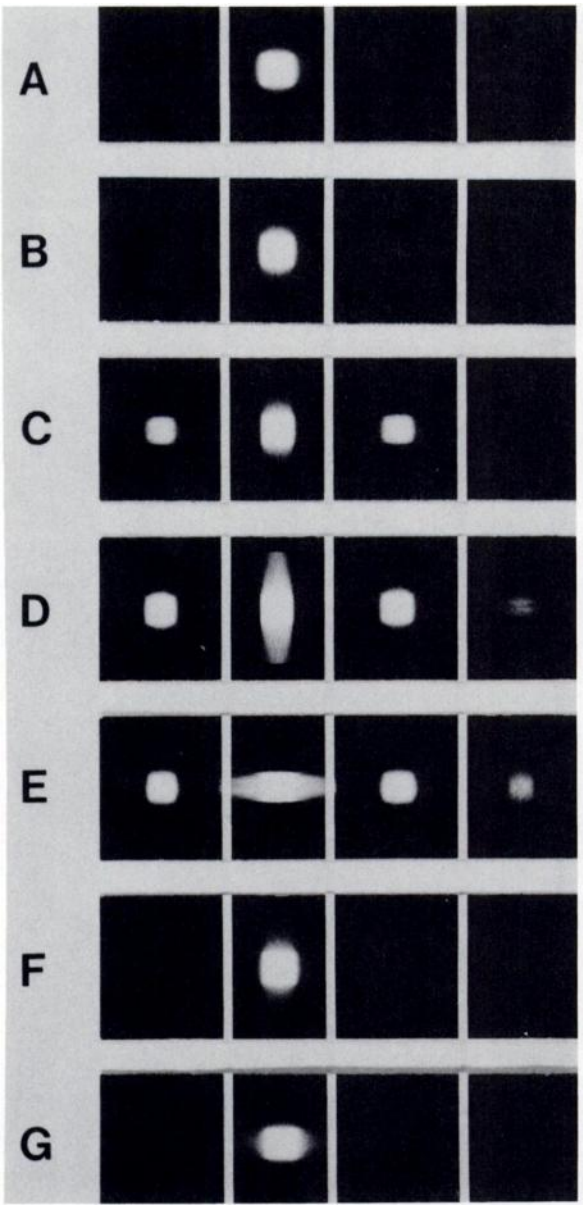

FIGURE 3
Reconstructed volume images resulting from the box phantom simulations. Each set of four images displayed horizontally is a series of contiguous, 2-mm thick axial slices through the volume image. The simulated data shown are as follows: (A) projection method, (x, y) = (0 cm, 0 cm); (B) projection method, (x, y) = (5 cm, 0 cm); (C) projection method, (x, y) = (10 cm, 0 cm); (D) projection method, (x, y) = 20 cm, 0 cm); (E) projection method, (x, y) = (0 cm, 20 cm); (F) event-by-event backprojection method, (x, y) = (20 cm, 0 cm); (G) event-by-event backprojection method, (x, y) = (0 cm, 20 cm).

A graph of the count density, normalized by the total number of counts in the volume image, in a small region of interest within the box as a function of radial position of the box is shown in Figure 5. With the two-dimensional projection technique, the normalized count density drops significantly over the field of view

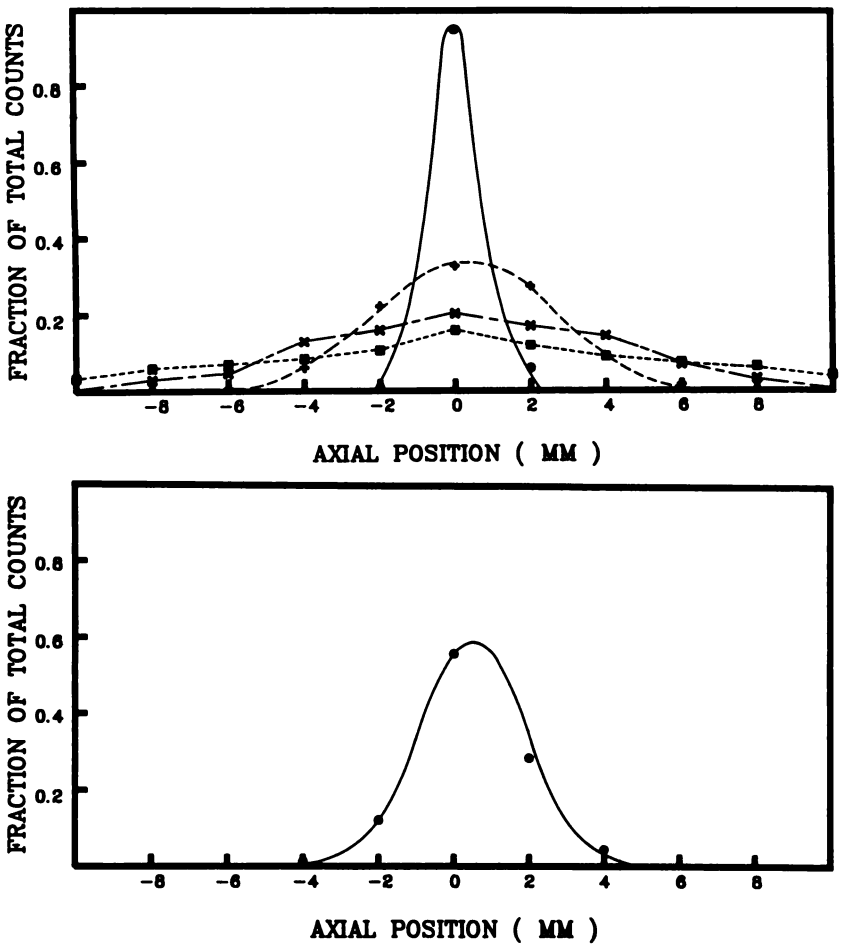

FIGURE 4
Plot of fraction of total volume counts in each slice as a function of slice position for the box phantom simulations. At the top are shown the results for the projection method with the following symbols: ——●—— (x, y) = (0 cm, 0 cm); —+— (x, y) = (5 cm, 0 cm); ·×· (x, y) = (10 cm, 0 cm); —■— (x, y) = (20 cm, 0 cm). At the bottom is the count profile for the event-by-event backprojection method. The results for all transverse locations of the box in the scanner were identical with this technique.

of the scanner to almost 10% of the central value at a radial distance of 20 cm. There is little difference in quantitative accuracy for objects moved in the x- and y-directions. With the event-by-event backprojection method the normalized count density remains constant out to 20 cm.

Brain Phantom

The images resulting from the simulation of a 2-mm-thick distribution of fluorodeoxyglucose in a normal brain centered in the scanner are shown in Figure 6 for 2-mm-thick slices. The slice of highest intensity is approximately centered upon the object. Serious image reconstruction artifacts are revealed for the two-dimensional projection method. The image corresponding to the central slice shows low resolution near the edges of the brain with an intense band of activity around the border of the phantom. The adjacent slices have excellent resolution of the edge structures, but the central regions are completely lost. Images generated with the event-by-event backprojection method show no visible artifacts for the plane containing the phantom and a low-intensity, generally featureless background in adjacent planes.

The quantitative accuracy of small areas in the brain phantom was assessed by drawing a profile through the center of the image in the central 2-mm slice (Fig. 7). The profile through the center of the simulated phantom which has a gray matter/white matter ratio of 4.0 and a gray matter/background ratio of infinity is shown for comparison. These results indicate serious inaccuracies arising from both methods of treating the axial information from very thin objects. The results are improved dramatically, however, by selecting a slice thickness of 6 mm instead of 2 mm. In the thicker slices, essentially all reconstructed information is contained in a single slice, and no artifacts are observed in the reconstructed images with either method.

Spheres

The images for 2-mm-wide slices resulting from the simulation of the complex sphere phantom are shown in Figure 8. No serious image artifacts are visible with either method. The large central sphere, with a diameter of 40 mm, extends over ~20 2-mm-wide slices with no hint of axial smearing. The other spheres which are not centered in the scanner are similarly well-reproduced, although with the two-dimensional projection approach, the smaller spheres appear oblong rather than circular. Overall, the volume image produced by either technique appears to be an accurate representation of the original phantom.

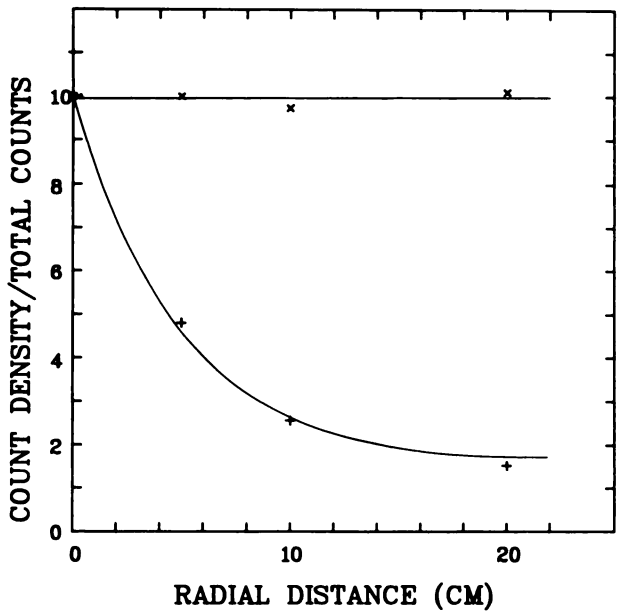

FIGURE 5
Plot of count density normalized by total volume counts in a small region of interest drawn inside the reconstructed box phantom as a function of radial distance of the box from the center of the scanner. The lower curve (+) was obtained using the projection method; the upper curve (x) resulted from the event-by-event backprojection technique.

DISCUSSION

With the two-dimensional projection approximation, objects having sharp axial boundaries show serious image artifacts and loss of quantitative accuracy. These problems are due to axial mispositioning caused by the underlying assumption that all coincidence lines are perpendicular to the scanner axis at an axial location midway between the two measured axial positions. As the source is moved radially off-center, oblique coincident rays will not have an average axial position at the actual axial location of object. The slices at the average axial positions will be given activity at the same transverse position as the "correct" slice, thus removing activity from the proper slice and smearing it over many slices. The axial mispositioning also affects the transverse distribution of rays, since not all projection angles are represented in all slices with the same probability. Therefore, upon backprojection the contributions of rays at certain angles will be missing, depending upon the location of the source in the scanner.

The qualitative and quantitative artifacts are reduced significantly if the object has a smooth axial gradient. Although a given point of activity is still blurred axially,

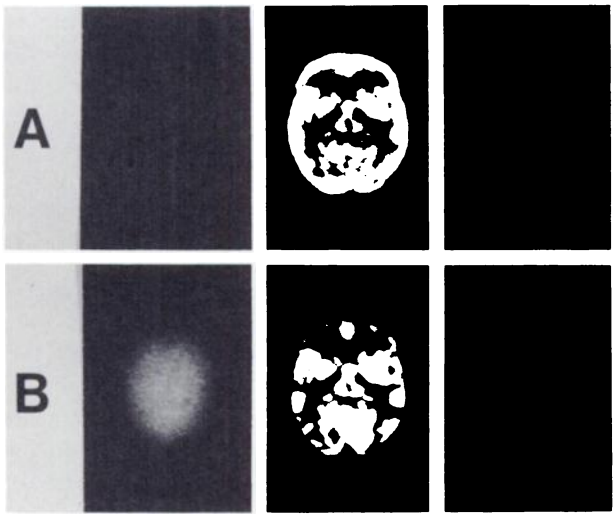

FIGURE 6
Reconstructed images resulting from simulation of digitized brain phantom. Each set of three images displayed horizontally is a series of contiguous, 2-mm-thick slices through the volume image. The projection method was used in (A), and the event-by-event backprojection technique was used in (B).

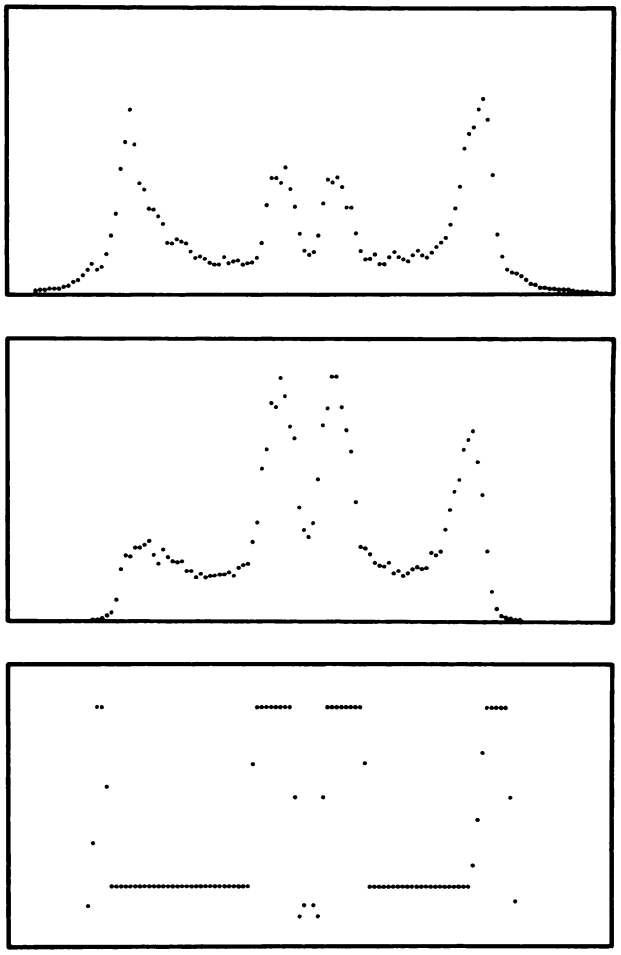

FIGURE 7
Profiles drawn through simulated brain phantom images. The profiles were drawn horizontally through the central 2-mm-thick slice, one-third of the way down the image. The profiles are ordered: (A) projection method, (B) event-by-event backprojection technique, (C) original digitized distribution. The original distribution contained a gray matter:white matter:background ratio of 4:1:0.

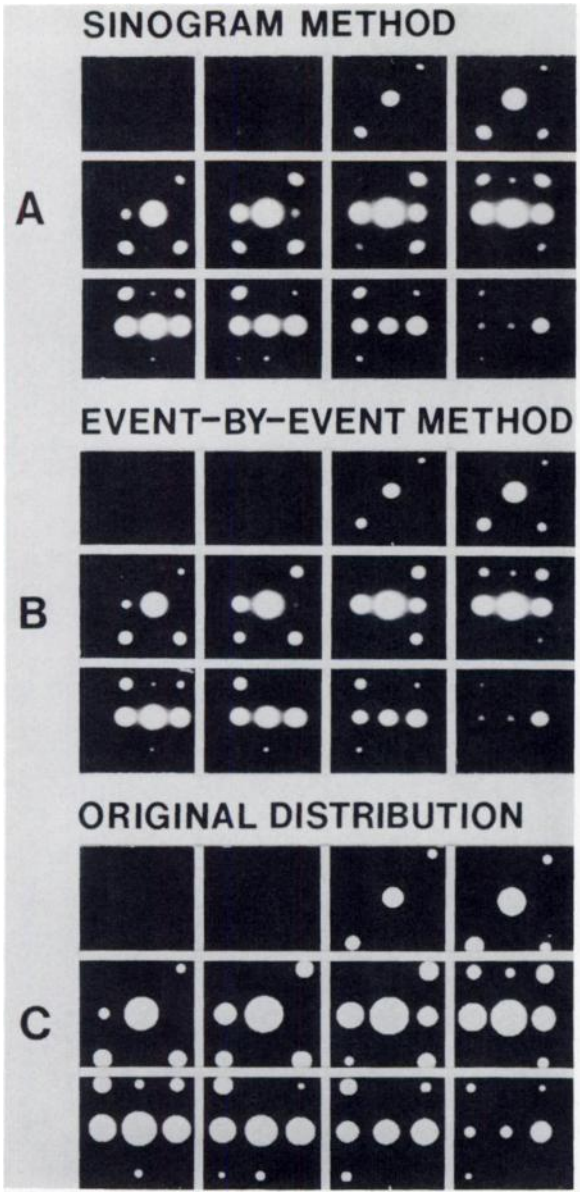

FIGURE 8
Reconstructed volume images resulting from simulation of complex sphere phantom. Each set of 12 images displayed is a series of 2-mm-thick slices through the volume image. The projection method was used in (A); the event-by-event backprojection technique was used in (B). The original distribution is shown in (C) for comparison. The original distribution appears larger than the reconstructed results due to a slight change of scale during the reconstruction process.

there is a high probability that there is a point of activity at the same radial location in a nearby slice which will be blurred into the first slice. The combined effect of the axial smearing of many point sources is a partial compensation for the loss out of one slice by losses out of others into that slice, with the degree of compensation dependent upon the sharpness of the object's boundary. The transverse spreading seen as the box was moved off-center is also compensated for by projections from other slices. With the event-by-event backprojection technique both the axial and radial locations are altered. By ignoring the axial correlations of the back-projected data in treating the slices independently during reconstruction, a point of activity gives rise to a low-intensity background around the source location in nearby slices. In objects with sharp axial gradients these "halo" artifacts are seen as bands of activity in neighboring slices. As slice thickness increases, the artifact is less noticeable due to the low intensity of the "halo" relative to the central intensity of the object. As with the projection method, axial problems are more pronounced with objects having sharp axial boundaries and are greatly reduced for spherical objects with axial extensions of several slices.

It is interesting to note that most of the quantitative and qualitative errors represent a serious problem only for 2-mm-thick slices and a large axial acceptance angle. In most practical situations, the slice thickness will be larger than 2 mm to obtain acceptable statistical accuracy, and the acceptance angle will likely be restricted to $<13°$ in order to keep scattered radiation reaching the detectors to an acceptably low level. Particularly if the event-by-event backprojection technique is used, errors introduced by the use of a two-dimensional instead of a fully three-dimensional reconstruction algorithm are likely going to be small relative to other sources of error.

ACKNOWLEDGMENTS

This work was supported by the U.S. Department of Energy under Grant DOE-AC02-80EV10402 and by the National Institutes of Health under Grant NIH NS14867. The authors thank Drs. Joel S. Karp, Gabor Herman and Robert Lewitt for helpful discussions.

REFERENCES

1. Pelc NJ. A generalized filtered backprojection algorithm for three dimensional reconstruction. M.S. Thesis: Harvard University, Cambridge, MA, 1979.
2. Daube-Witherspoon ME, Muehllehner G. An iterative image space reconstruction algorithm suitable for volume ECT. *IEEE Trans Med Imag* 1986; MI-5:61–66.
3. Colsher JG. Fully three-dimensional positron emission tomography. *Phys Med Biol* 1980; 25:103–115.
4. Townsend D, Schorr B, Jeavons A. Three-dimensional image reconstruction for a positron camera with limited angular acceptance. *IEEE Trans Nucl Sci* 1980; NS-27:463–470.
5. Cho ZH, Ra JB, Hilal SK. True three-dimensional reconstruction (TTR)—Application of algorithm toward full utilization of oblique rays. *IEEE Trans Med Imag* 1983; MI-2:6–18.
6. Chu G, Tam K. Three-dimensional imaging in the positron camera using Fourier techniques. *Phys Med Biol* 1977; 22:245–265.
7. Atkins F, Muehllehner G, Harper PV. Positron emission computed tomography using large area detectors.

In: Information processing in medical imaging. ORNL/BCTIC-2. 1978:196–213.
8. Schorr B, Townsend D, Clack R. A general method for three-dimensional filter computation. *Phys Med Biol* 1983; 28:1009–1019.
9. Ra JB, Lim CB, Cho ZH, et al. A true three-dimensional reconstruction algorithm for the spherical positron emission tomography. *Phys Med Biol* 1982; 27:37–50.
10. Pelc NJ, Chesler DA. Utilization of cross-plane rays for three-dimensional reconstruction by filtered back-projection. *J Comput Assist Tomogr* 1979; 3:385–395.
11. Colsher JG. Iterative three-dimensional image reconstruction from tomographic projections. *Comput Graph Image Process* 1977; 6:513.
12. Altschuler MD, Censor Y, Eggermont PPB, et al. Demonstration of a software package for the reconstruction of the dynamically changing structure of the human heart from cone beam x-ray projections. *J Med Syst* 1980; 4:289–304.
13. Muehllehner G, Colsher JG, Lewitt RM. A hexagonal bar positron camera: problems and solutions. *IEEE Trans Nucl Sci* 1983; NS-30:652–660.
14. Muehllehner G, Karp JS. A positron camera using position-sensitive detectors: PENN-PET. *J Nucl Med* 1986; 27:90–98.
15. Karp JS, Muehllehner G, Beerbohm D, et al. Event localization in a continuous scintillation detector using digital processing. *IEEE Trans Nucl Sci* 1986; NS-33:550–555.
16. Shepp LA, Vardi Y. Maximum likelihood reconstruction for emission tomography. *IEEE Trans Med Imag* 1982; MI-1:113–122.
17. Floyd DE Jr, Jaszczak RJ, Coleman RE. Inverse Monte Carlo: a unified reconstruction algorithm for SPECT. *IEEE Trans Nucl Sci* 1985; NS-32:779–785.